



1 Satellite-based Estimation of the Impacts of Summertime Wildfires on
2 Particulate Matter Air Quality in United States

3 Zhixin Xue¹, Pawan Gupta^{2,3}, and Sundar Christopher¹

4 ¹Department of Atmospheric and Earth Science, The University of Alabama in Huntsville,
5 Huntsville, 35806 AL, USA

6 ²STI, Universities Space Research Association (USRA), Huntsville, 35806 AL, USA

7 ³NASA Marshall Space Flight Center, Huntsville, AL, 35806, USA

8 **Abstract**

9 Frequent and widespread wildfires in North Western United States and Canada has become
10 the “*new normal*” during the northern hemisphere summer months, which degrades particulate
11 matter air quality in the United States significantly. Using the mid-visible Multi Angle
12 Implementation of Atmospheric Correction (MAIAC) satellite-derived Aerosol Optical Depth
13 (AOD) with meteorological information from the European Centre for Medium-Range Weather
14 Forecasts (ECMWF) and other ancillary data, we quantify the impact of these fires on fine
15 particulate matter air quality (PM_{2.5}) in the United States. We use a Geographically Weighted
16 Regression method to estimate surface PM_{2.5} in the United States between low (2011) and high
17 (2018) fire activity years. Our results indicate that smoke aerosols caused significant pollution
18 changes over half of the United States. We estimate that nearly 29 states have increased PM_{2.5}
19 during the fire active year and 15 of these states have PM_{2.5} concentrations more than 2 times
20 than that of the inactive year. Furthermore, these fires increased daily mean surface PM_{2.5}
21 concentrations in Washington and Oregon by 38 to 259 $\mu\text{g m}^{-3}$ posing significant health risks
22 especially to vulnerable populations. Our results also show that the GWR model can be



23 successfully applied to PM_{2.5} estimations from wildfires thereby providing useful information for
24 various applications including public health assessment.

25 **1. Introduction**

26 The United States (US) Clean Air Act (CAA) was passed in 1970 to reduce pollution levels
27 and protect public health that has led to significant improvements in air quality (Hubbell et al.,
28 2010; Samet, 2011). However, the northern part of the US continues to experience an increase in
29 surface PM_{2.5} due to fires in North Western United States and Canada (hereafter NWUSC)
30 especially during the summer months and these aerosols are a new source of ‘pollution’ (Dreessen
31 et al., 2016). The smoke aerosols from these fires increase fine particulate matter (PM_{2.5})
32 concentrations and degrade air quality in the United States (Miller et al., 2011). Moreover several
33 studies have shown that from 2013 to 2016, over 76% of Canadians and 69% of Americans were
34 affected by wildfire smoke (Munoz-Alpizar et al., 2017). Although wildfire pre-suppression and
35 suppression costs have increased, the number of large fires and the burnt areas in many parts of
36 western Canada and the United States have also increased. (Hanes et al., 2019; Tymstra et al.,
37 2019). Furthermore, in a changing climate, as surface temperature increases and humidity
38 decreases, the flammability of land cover also increases, and thus accelerate the spread of wildfires
39 (Melillo et al., 2014; Coogan et al, 2019). The accumulation of flammable materials like leaf litter
40 can potentially trigger severe wildfire events even in those forests that hardly experience wildfires
41 (Calkin et al., 2015; Hessburg et al., 2015; Stephens, 2005). .

42 Wildfire smoke exposure can cause small particles to be lodged in lungs that may lead to
43 exacerbations of asthma chronic obstructive pulmonary disease (COPD), bronchitis, heart disease
44 and pneumonia (Cascio, 2018). According to a recent study, a 10 $\mu\text{g m}^{-3}$ increase in PM_{2.5} is
45 associated with a 12.4% increase in cardiovascular mortality (Kollanus et al., 2016). In addition,



46 exposure to wildfire smoke is also related to massive economic costs due to premature mortality,
47 loss of workforce productivity, impacts on the quality of life and compromised water quality
48 (Meixner and Wohlgemuth, 2004).

49 Surface PM_{2.5} is one of the most commonly used parameters to assess the health effects
50 of ambient air pollution. Since surface monitors are limited, satellite data has been used with
51 numerous ancillary data sets to estimate surface PM_{2.5} at various spatial scales. Several techniques
52 have been developed to estimate surface PM_{2.5} using satellite observations from regional to global
53 scales including simple linear regression, multiple linear regression, mixed-effect model, chemical
54 transport model (scaling methods), geographically weighted regression (GWR), and machine
55 learning methods (see Hoff and Christopher, 2009 for a review). The commonly used global
56 satellite data product is the 550nm (mid-visible) aerosol optical depth (AOD) which is a unitless
57 columnar measure of aerosol extinction (Wang and Christopher, 2006). Simple linear regression
58 method uses satellite AOD as the only independent variable, which shows limited predictability
59 compared to other method and correlation coefficients vary from 0.2 to 0.6 from the Western to
60 Eastern United States (Zhang et al., 2009). Multiple linear regression method uses meteorological
61 variables along with AOD data, and the prediction accuracy varies with different conditions
62 including the height of boundary layer and other meteorological conditions (Liu, et al, 2005; Gupta
63 and Christopher, 2009b). For both univariate model and multi-variate models, AOD shows
64 stronger correlation with PM_{2.5} during-fire episodes compared to pre-fire and post-fire periods
65 (Mirzaei et al., 2018). Chemistry transport models (CTM) that scale the satellite AOD by the ratio
66 of PM_{2.5} to AOD simulated by models can provide PM_{2.5} estimations without ground
67 measurements, which are different than other statistical methods (Donkelaar et al, 2006). However,
68 the CTM models that depend on reliable emission data usually show limited predictability at



69 shorter time scales, and is largely useful for studies that require annual averages (Hystad et al.,
70 2012).

71 The relationship among PM_{2.5}, AOD and other meteorological variables is not spatially
72 consistent (Hoff and Christopher, 2009; Hu, 2009) and therefore methods that consider spatial
73 variability can replicate surface PM_{2.5} with higher accuracy. One such method is the GWR, which
74 is a non-stationary technique that models spatially varying relationships by assuming the
75 coefficients in the model are functions of locations (Brunsdon et al., 1996; Fotheringham et al.,
76 1998, 2003). In 2009, satellite-retrieved AOD was introduced in the GWR method to predict
77 surface PM_{2.5} (Hu, 2009) followed by the use of meteorological parameters and land use
78 information (Hu et al., 2013). Other studies (Ma et al., 2014; You et al., 2016) successfully applied
79 GWR model in estimating PM_{2.5} using AOD and meteorological features as predictors. Similar
80 to most statistical methods, however, the GWR relies on adequate number and density of surface
81 measurements (Chu et al., 2016; Gu, 2019), underscoring the importance of adequate ground
82 monitoring of surface PM_{2.5}.

83 In this paper, we use satellite data products from the Moderate Resolution Imaging
84 Spectroradiometer (MODIS) and surface PM_{2.5} data combined with meteorological and other
85 ancillary information to develop and use the GWR method to estimate PM_{2.5}. The use of the GWR
86 method is not novel and we merely use an existing method to apply this towards surface PM_{2.5}
87 estimations for forest fires. We calculate the change in PM_{2.5} between a high fire activity (2018)
88 with low fire activity (2011) periods during summer to assess the role of NWUSC wildfires on
89 surface PM_{2.5} in the United States. The paper is organized as follows: We describe the data sets
90 used in this study followed by the GWR method. We then describe the results and discussion
91 followed by a summary with conclusions.



92 **2. Data**

93 A 17-day period (August 9th to August 25th) in 2018 (high fire activity) and 2011 (low fire
94 activity) was selected based on analysis of total fires (details in methodology section) to assess
95 surface PM_{2.5} (Table 1).

96 **2.1 Ground level PM_{2.5} observations:** Daily surface PM_{2.5} from the Environment Protection
97 Agency (EPA) are used in this study. These data are from Federal Reference Methods (FRM),
98 Federal Equivalent Methods (FEM), or other methods that are to be used in the National Ambient
99 Air Quality Standards (NAAQS) decisions. A total of 1003 monitoring sites in the US are included
100 with 949 of those having valid observations in the study period in 2018, and a total of 873 sites
101 with 820 having valid observations in the study period in 2011. PM_{2.5} values less than 2 μg m⁻³
102 are discarded since they are lower than the established detection limit (Hall et al., 2013).

103 **2.2 Satellite Data:** The MODIS mid visible AOD from the Multi-Angle Implementation of
104 Atmospheric Correction (MAIAC) product (MCD19A2 Version 6 data product) is used in this
105 study. We used MAIAC retrieved Terra and Aqua MODIS AOD product at 1 km pixel resolution
106 (Lyapustin et al., 2018) and different orbits are averaged to obtain mean daily values. Validation
107 with AERONET studies show that 66% of the MAIAC AOD data agree within ±0.5~±0.1 AOD
108 (Lyapustin et al., 2018). Largely due to cloud cover, grid cells may have limited number of AOD
109 observations within a certain period. On average, cloud free AOD data are available about 40% of
110 the time during August 9th to August 25th in 2018 when fires were active in the region bounded by
111 25~50°N, 65~125°W.

112 We also use the MODIS level-3 daily FRP (MCD14ML) product which combines Terra
113 and Aqua fire products to assess wildfire activity. The fire radiative energy indicates the rate of



114 combustion and thus FRP can be used for characterizing active fires (Freeborn et al, 2014). For
115 purposes of the study we sum the FRP within every $2.3^{\circ} \times 3.5^{\circ}$ box to represent the total fire activity
116 in different locations.

117 **2.3 Meteorological data:** Meteorological information including boundary layer height (BLH), 2m
118 temperature (T2M), 10m wind speed (WS), surface relative humidity (RH) and surface pressure
119 (SP) are obtained from the European Centre for Medium-Range Weather Forecasts (ECMWF)
120 reanalysis (ERA5) product, with a spatial resolution of 0.25 degrees and temporal resolution of 1
121 hour and is matched temporally with the satellite overpass time. The BLH can provide information
122 of aerosol layer height as aerosols are often found to be well-mixed within the boundary layer
123 (Gupta and Christopher, 2009b). A higher RH will increase the hygroscopicity, change scattering
124 properties of certain aerosol types and can lead to a higher AOD value (Zheng et al., 2017). In
125 addition, high surface temperatures can also accelerate the formation of secondary particles in the
126 atmosphere.

127 **2.4 Land cover and population data:** Land cover and population density is highly related to
128 anthropogenic aerosol emissions, which also affects surface PM_{2.5}. Land cover information from
129 the European Space Agency (ESA) with a spatial resolution of 300m and temporal resolution of
130 one year (ESA, 2017) and population data from 'Gridded Population of the World', v4 (GPWv4)
131 with a spatial resolution of 5 km are used as variables for the GWR method used in this study. The
132 ESA land cover product uses global time series input datasets acquired by the Envisat Medium
133 Resolution Imaging Spectrometer (MERIS) and from the SPOT-Vegetation (SPOT-VGT) sensors.
134 The global land surface reflectance values are produced from the MERIS level-1 dataset, which
135 along with SPOT-VGT S1 (daily synthesis product) are used as input to the classification module



136 and interprets into land cover classes. The population data uses results of the 2010 Population and
137 Housing Census as input data.

138 **3. Methodology**

139 To assess the impact of NWUSC fires on PM_{2.5} in the United States, we first estimate the
140 PM_{2.5} over the study region during a time period with high fire activity (2018). We then use the
141 same method during a year with low fire activity (2011) to compare the differences between the
142 two years. The two years are selected based on the total FRP in August calculated within Canada
143 (49~60°N, 55~135°W) and Northwestern (NW) US (35~49°N, 105~125°W). Table 2 shows the
144 total FRP in Canada and Northwestern US in August from 2010 to 2018. The total FRP in the two
145 regions is lowest in 2011 and highest in 2018 during the 9 years, which provides the basis for the
146 study. In order to create a 0.1° surface PM_{2.5}, the GWR model is used to estimate the relationships
147 of PM_{2.5} and AOD. Detailed processing steps for GWR model are shown in Figure 1.

148 **3.1 Data preprocessing:** The first step is to resample all datasets to a uniform spatial resolution
149 by creating a 0.1° resolution grid covering the Continental United States. During this process, we
150 collocate the PM_{2.5} data and average the values if there is more than one value in one grid. Then
151 the MAIAC AOD, land cover and population data are averaged into 0.1° grid cells. Meteorological
152 datasets are also resampled to the 0.1° grid cells by applying the inverse distance method.

153 **3.2 Time selecting & averaging:** Next we select data where AOD and ground PM_{2.5} are both
154 available (AOD > 0 and PM_{2.5} > 2.0 μg m⁻³) and average them for the study period. This is to
155 ensure that the AOD, PM_{2.5} and other variables match with each other, because PM_{2.5} is not a
156 continuous measurement for some sites and AOD have missing values due to cloud cover and



157 other reasons. Therefore, it is important to use data from days where both these measurements are
158 available to avoid sampling biases.

159 **3.3 GWR model development and validation:** The strength of GWR is its ability to model
160 complex spatially varying relationships which is well suited for assessing surface PM_{2.5} and
161 ancillary data. It is an extension of the least regression method but it allows the relationship
162 between dependent and independent variables to vary by location and also accounts for spatial
163 auto-correlation of variables. Since the GWR fits a separate equation for each grid, a bandwidth
164 must be selected for each location. In this study we use the commonly used Adaptive bandwidth
165 method selected by the Akaike's Information Criterion (AIC) is used for the GWR model (Loader,
166 1999). For locations that already have PM_{2.5} monitors, we calculate the mean AOD of a 0.5×0.5°
167 box centered at the ground location and estimate the GWR coefficients (β) for AOD and
168 meteorological/land cover variables to estimate PM_{2.5}. The model structure can be expressed as:

$$169 \quad PM_{2.5i} = \beta_{0,i} + \beta_{1,i}AOD_i + \beta_{2,i}BLH_i + \beta_{3,i}T2M_i + \beta_{4,i}U10M_i + \beta_{5,i}RH_{sfc_i} + \beta_{6,i}SP_i + \beta_{7,i}LC_i \\ 170 \quad \quad \quad + \beta_{8,i}POP_i + \varepsilon_i$$

171 where $PM_{2.5i}$ ($\mu g m^{-3}$) is the selected ground-level PM_{2.5} concentration at location i ;
172 $\beta_{0,i}$ is the intercept at location i ; $\beta_{1,i} \sim \beta_{8,i}$ are the location-specific coefficients; AOD_i is the
173 resampled AOD selected from MAIAC daily AOD data at location i ;
174 $BLH_i, T2M_i, U10M_i, RH_{sfc_i}, SP_i$ are selected meteorological parameters (BLH, T2M, WS, RH and
175 PS) at location i ; LC_i is the resampled land cover data at location i ; POP_i ($person/km^2$) is the
176 resampled population density at location i ; and ε_i is the error term at location i .

177 We perform the Leave One Out Cross Validation (LOOCV) to test the model predictive
178 performance (Kearns and Ron, 1999). Since the GWR model relies on adequate number of



179 observations, the prediction accuracy will be lower if we preserve too much data for validation.
180 Therefore, we choose the LOOCV method, which preserve only one data point for at a time for
181 validation and repeat the process until all the data are used. In addition, R^2 and RMSE are
182 calculated for both model fitting and model validation process to detect overfitting. Model
183 overfitting will lead to low predictability, which means it fits too close to the limited number of
184 data to predict for other places and will cause large bias.

185 **3.4 Model prediction:** While predicting the ground-level PM_{2.5} for unsampled locations, we
186 make use of the estimated parameters for sites within a 5° radius to generate new slopes for
187 independent variables based on the spatial weighting matrix (Brunsdon et al., 1996). The closer to
188 the predicted location, the closer to 1 the weighting factor will be, while the weighting factor for
189 sites further than the 5° in distance is zero. It is important to note that AOD and other independent
190 variables used for prediction in this step are averaged values for days that have valid AOD, which
191 is different from the data used in the fitting process since PM_{2.5} is not measured every day in all
192 locations.

193 **4. Results and Discussion**

194 We first discuss the surface PM_{2.5} for a few select locations that are impacted by fires
195 followed by the spatial distribution of MODIS AOD and the FRP for August 2018. We then assess
196 the spatial distribution of surface PM_{2.5} from the GWR method. The validation of the GWR
197 method is then discussed. To further demonstrate the impact of the NWUSC fires on PM_{2.5} air
198 quality in the United States, we show the spatial distribution of the difference between August
199 2018 and August 2011. We further quantify these results for ten US EPA regions.

200



201 **4.1 Descriptive statistics of satellite data and ground measurements**

202 The 2018 summertime Canadian wildfires started around the end of July in British
203 Columbia and continued until mid-September. The fires spread rapidly to the south of Canada
204 during August, causing high concentrations of smoke aerosols to drift down to the US and affecting
205 particulate matter air quality significantly. From late July to mid-September, wildfires in the
206 northwest US that burnt forest and grassland also affected air quality in the United States but the
207 number and intensity of fires were less than the fires in Canada (Figure 2). Starting with the Cougar
208 Creek Fire, then Crescent Mountain and Gilbert Fires, different wildfires in in NWUSC caused
209 severe air pollution in various US cities. Figure 2a shows the rapid increase in PM_{2.5} of selected
210 US cities from July 1st to August 31st, due to the transport of smoke from these wildfires. For all
211 sites, July had low PM_{2.5} concentrations ($<10 \mu\text{g m}^{-3}$) and rapidly increased with fire activity.
212 Calculating only from the EPA ground observations, the mean PM_{2.5} of the 17 days for the whole
213 US is $13.7 \mu\text{g m}^{-3}$ and the mean PM_{2.5} for Washington (WA) is $40.6 \mu\text{g m}^{-3}$, which indicates
214 that the PM pollution is concentrated in the northwestern US for these days. This trend is obvious
215 when comparing the mean PM_{2.5} of all US stations (black line with no markers) and the mean
216 PM_{2.5} of all WA stations (grey line with no markers). Ground-level PM_{2.5} reaches its peak
217 between August 17th-21st and daily PM_{2.5} values during this time period far exceeds the 17-day
218 mean PM_{2.5}. For example, mean PM_{2.5} in WA on August 20th is $86.75 \mu\text{g m}^{-3}$, which is more
219 than two times the 17-day average of this region. On August 19th, Omak which is located in the
220 foothills of the Okanogan Highlands in WA had PM_{2.5} values exceed $250 \mu\text{g m}^{-3}$. According to
221 a review of US wildfire caused PM_{2.5} exposures, 24-h mean PM_{2.5} concentrations from wildfires
222 ranged from 8.7 to $121 \mu\text{g m}^{-3}$, with a 24 h maximum concentration of $1659 \mu\text{g m}^{-3}$ (Navarro et
223 al., 2018).



224 The spatial distribution of MAIAC AOD shown in Figure 2b indicates that the smoke from
225 Canada is concentrated mostly in Northern US states such as WA, Oregon, Idaho, Montana, ND
226 and Minnesota. The black arrows show the mean 800hPa-level mean wind for 17 days, and the
227 length of the arrow represents the wind speed in ms^{-1} . Also shown in Figure 2b are wind speeds
228 close to the fire sources which are about $4\text{--}5 \text{ ms}^{-1}$, and according to the distances and wind
229 directions, it can take approximately 28~36 hours for the smoke to transport southeastward to
230 Washington state. Then the smoke continues to move east to other northern states such as Montana
231 and North Dakota. In addition, the grey circle represents the total fire radiative power (FRP) of
232 every 2.3×3.5 -degree box. The reason for not choosing a smaller grid for the FRP is to not clutter
233 Figure 2b with information from small fires. The bigger the circle is, the stronger the fire in that
234 grid. It is clear that the strongest fires in 2018 are located in the Tweedsmuir Provincial Park of
235 British Columbia in Canada (53.333N , 126.417W). The four separate lightning-caused wildfires
236 burnt nearly 301,549 hectares of the boreal forest. The total FRP of August 2018 in Canada is
237 about 5362 (*1000 MW), while the total FRP of August 2011 in Canada is 48 (* 1000 MW). The
238 2011 fire was relatively weak compared to the 2018 Tweedsmuir Complex fire and we therefore
239 use the 2011 air quality data as a baseline to quantify the 2018 fire influence on $\text{PM}_{2.5}$ in the
240 United States.

241 **4.2 Model Fitting and validation**

242 The main goal for using GWR model is to help predict the spatial distribution of $\text{PM}_{2.5}$
243 for places with no ground monitors while leveraging the satellite AOD and therefore it is important
244 to ensure that the model is robust. Figure 3a and 3b show the results for 2018 for GWR model
245 fitting for the entire US and the LOOCV models respectively. The color of the scatter plots
246 represents the probability density function (PDF) which calculates the relative likelihood that the



247 observed ground-level PM_{2.5} would equal the predicted value. The lighter colors indicate more
248 data points with a higher correlation. The model fitting process estimates the slope for each
249 variable and therefore the model can be fitted close to the observed PM_{2.5} and using this estimated
250 relationship we are able to assess surface PM_{2.5} using other parameters at locations where PM_{2.5}
251 monitors were not available. The LOOCV process tests the model performance in predicting
252 PM_{2.5}. If the results of LOOCV has a large bias from the model fitting, then the predictability of
253 the model is low. Higher R² difference and RMSE difference value indicate that the model is
254 overfitting the data and therefore not suitable. The R² for the model fitting is 0.84, and the R² for
255 the LOOCV is 0.804; the RMSE for the GWR model fitting is 3.4 μg m⁻³, and for LOOCV the
256 RMSE is 3.77 μg m⁻³. There are minor differences between fitting R² and validation R² (0.036)
257 and between fitting RMSE and validation RMSE (0.37 μg m⁻³) suggesting that the model is not
258 over-fitting and has stable predictability further indicating that the model can predict surface
259 PM_{2.5} reliably. In addition, we also performed a 20-fold cross validation by splitting the dataset
260 into 20 consecutive folds, and each fold is used for validation while the 19 remaining folds form
261 the training set. The 20-fold cross validation has R² of 0.76 and RMSE of 4.15 μg m⁻³. The
262 increase/decrease in the cross validated R² and RMSE indicates the importance of sufficient data
263 used for fitting since a small decrease in the number of fitting data can reduce the model prediction
264 accuracy. Overall, the prediction error of the model is between 3~5 μg m⁻³, which is a reasonable
265 error range for 17-day average prediction of PM_{2.5}.

266 **4.3 Predicted PM_{2.5} Distribution**

267 The mean PM_{2.5} distributions over the United States shown in Figure 4a is calculated by
268 averaging the surface PM_{2.5} data from ground monitors for the 17 days, which matches well with
269 the GWR model-predicted PM_{2.5} distributions shown in Figure 4b. The model estimation extends



270 the ground measurements and provide pollution assessments across the entire nation. Comparing
271 the AOD map (Figure 2b) with the PM_{2.5} estimations (Figure 4b), demonstrates the differences
272 between columnar and surface-level pollution. Differences between the AOD and PM_{2.5}
273 distributions are due to various reasons including 1) Areas with high PM_{2.5} concentrations in
274 figure 4b correspond to low AOD values in figure 2b (Southern California, Utah, and southern
275 US); 2) and high AOD regions in figure 2b correspond to low PM_{2.5} concentrations in figure 4b
276 (Minnesota). The first situation usually occurs at the edge of polluted areas that are relative far
277 from the fire source, which is consistent with previous studies that reported smaller particles (<10
278 μg) are able to travel longer distances compared to large particles (>10 μg) (Gillies et al., 1996),
279 and that larger particles tend to settle closer to their source (Sapkota et al., 2005; Zhu et al., 2002).

280 We use the same method for August 9th to August 25th in 2011 that had low fire activity,
281 ensuring consistency for estimating coefficients for different variables for 2011. Figure 4c shows
282 the difference in spatial distribution of mean ground PM_{2.5} of the 17 days between 2018 and 2011.
283 High values of PM_{2.5} differences are in the Northwestern and central parts of the United States
284 with the Southern states having very little impact due to the fires. Of all the 48 states within the
285 study region, there are 29 states that have a higher PM_{2.5} value in 2018 than 2011, and 15 states
286 have 2018 PM_{2.5} value more than two times their 2011 value (shown in table 3). The mean PM_{2.5}
287 for WA increases from 5.87 in 2011 to 47.1 $\mu\text{g m}^{-3}$ in 2018, which is about 8 times more than
288 2011 values. The PM_{2.5} values in Oregon increases from 4.97 (in 2011) to 33.1 $\mu\text{g m}^{-3}$ in 2018,
289 which is nearly seven times more than in 2011. For states from Montana to Minnesota, the mean
290 PM_{2.5} decreases from east to west, which reveals the path of smoke transport. As shown in Figure
291 4c, there is a clear transport path of smoke from North Dakota all the way to Texas. Along the
292 path, smoke increases PM_{2.5} concentrations by 173% in North Dakota and 26.2% in Texas. Smoke



293 aerosols transported over long distances contains fine fraction PM which significantly affect the
294 health of children, adults, and vulnerable groups.

295 Figure 5 shows the mean PM_{2.5} predicted from the GWR model of different EPA regions
296 for the 17 days in 2011 and 2018 (Hawaii and Alaska are not included). The most influenced region
297 is region 10, which has a 2018 mean PM_{2.5} value of $34.7 \mu\text{g m}^{-3}$ that is 6 times larger than the
298 values in 2011 ($5.8 \mu\text{g m}^{-3}$) values. The PM_{2.5} of EPA regions 8 and 9 have 2.7 and 2.5 times
299 increase in 2018 compared to 2011. Region 1~4 have lower PM_{2.5} in 2018 compared to 2011
300 possibly due to Clean Air Act initiatives, absence of any major fire activities and therefore further
301 away for transported aerosols. The emission reduction improves the US air quality and lower the
302 PM_{2.5} every year, but 6 out of 10 EPA regions show significant increases in PM_{2.5} during the
303 study period, which indicates that the long-range transported wildfire smoke has become the new
304 major pollutant in the US.

305 4.4 Estimation of Canadian fire pollution

306 To evaluate the pollution caused only from Canadian fires, we did a rough assessment
307 according to the total FRP and PM_{2.5} values. There are three states in the US have wildfires during
308 the study period: California, Washington and Oregon, and they have total FRP of 1186, 518 and
309 439 (*1000 MW) respectively. Assuming that California was only influenced by the local fires,
310 then fires of 1186 (*1000 MW) cause $13 \mu\text{g m}^{-3}$ increase in PM_{2.5}. Accordingly, wildfires in
311 Washington and Oregon State will cause 6 and $5 \mu\text{g m}^{-3}$ increase in state mean PM_{2.5}. Therefore,
312 Canadian fires caused PM_{2.5} increase in Washington and Oregon is about 35 and $23 \mu\text{g m}^{-3}$.
313 Since the FRP of Canadian wildfires are approximately 5 times larger than that of the California
314 fires, which is the strongest fire in US, we assume the pollution affecting the states located in the



315 downwind directions other than the three states are mainly coming from Canadian wildfires. States
316 with no local fires such as Montana, North Dakota, South Dakota and Minnesota have PM_{2.5}
317 increase of 18.31, 12.8, 10.4 and 10.13 $\mu\text{g m}^{-3}$. The decrease of these numbers reveal that the
318 smoke is transport in a SE direction. This influence of Canadian wildfires on US air quality is only
319 a rough quantity estimation, thus additional work is needed for understand long-range transport
320 smoke pollution and its impact on public health. One way to do this would be assessing the
321 difference of pollution by turning on and off US fires in chemistry models.

322 **4.4 Model uncertainties**

323 There are various sources of uncertainties and limitations for studies that use satellite data
324 to estimate surface PM_{2.5} concentrations. Since wildfires develop quickly it is important to have
325 continuous observations to capture the rapid changes. This study uses polar orbiting high-quality
326 satellite aerosol products, but the temporal evolution can only be estimated by geostationary data
327 sets. Although satellite observations have excellent spatial coverage, missing data due to cloud
328 cover is a limitation. As discussed in the paper, the prediction error (RMSE) of the model is
329 between 3~5 $\mu\text{g m}^{-3}$. The GWR model is largely influenced by the distribution of ground stations,
330 and the prediction error will be different in different places due to unevenly distributed PM_{2.5}
331 stations. For locations that have a dense ground-monitoring distribution, the prediction error will
332 be low, while the prediction error will be relative larger at other places with sparse surface stations.
333 Although there are obvious limitations, complementing surface data with satellite products and
334 meteorological and other ancillary information in a statistical model like the GWR has provided
335 robust results for estimating surface PM_{2.5} from wildfires. We also note that we did not consider
336 some variables used in other studies such as NDVI, forest cover, vegetation type, industrial
337 density, visibility and chemical constituents of smoke particles (Donkelaar et al., 2015; Hu et al.,



338 2013; You et al., 2015; Zou et al., 2016). While Land cover and land use information can improve
339 PM2.5 estimation predictability, redundant information such as NDVI can cause overfitting of
340 models. Therefore, in order to control the number of predictors used in the GWR model, we use
341 only one piece of land cover information. However, which of the land cover and land use
342 information performs better in predicting surface PM2.5 is still to be assessed in the future.
343 Visibility mentioned in some studies may improve the model performance, but unlike AOD, it has
344 limited measurement across the nation, which will restrict the applicability of training data.

345 **5. Summary and Conclusions**

346 We estimate the surface mean PM2.5 for 17 days in August for a high fire active year
347 (2018) and compare that with a low fire activity year using the Geographically Weighted
348 Regression (GWR) method to assess the increase in PM2.5 in the United States due to smoke
349 transported from fires. We selected the GWR because it has the capability to model complex
350 relationships that vary spatially. The difference in PM2.5 between the two years indicates that
351 more than half of the US states (29 states) are influenced by the NWUSC wildfires, and half of the
352 affected states have 17-day mean PM2.5 increases larger than 100% of the baseline value. The
353 peak PM2.5 during the wildfires can be much larger than the 17-day average and can affect
354 vulnerable populations susceptible to air pollution. Some of the most affected states are in
355 Washington, California, Wisconsin, Colorado and Oregon, all of which have populations greater
356 than 4 million. According to CDC (Centers for Disease Control and Prevention), 8% of the
357 population have asthma (CDC, 2011). Therefore, for asthma alone, there are about 3 million people
358 facing significant health issue due to the long-range transport smoke in these states.

359 For states that show decrease in PM2.5 due to the Clean Air Act, the mean decrease is
360 about 16% of the baseline after 7 years. This is consistent with EPA's report that there is a 23%



361 decrease of PM_{2.5} in national average from 2010 to 2019 (U.S. Environmental Protection Agency,
362 2019). Comparing with the dramatic increase (132%) caused by wildfires, pollution from the fires
363 is counteracting our effort on emission controls. Although wildfires are often episodic and short-
364 term, high frequency of fire occurrence and increasing longer durations of summertime wildfires
365 in recent years has made them now a long-term influence on public lives. Our results show a
366 significant increase of pollution in a short time period in most of the US states due to the NWUSC
367 wildfires, which affects millions of people. With wildfires becoming more frequent during recent
368 years, more effort is needed to predict and warn the public about the long-range transported smoke
369 from wildfires.

370

371 **Acknowledgements.**

372 Pawan Gupta was supported by a NASA Grant. MODIS data were acquired from the Goddard
373 DAAC. We thank all the data providers for making this research possible.

374 **References**

375 Brunson, C., Fotheringham, A.S., Charlton, M.E., 1996. Geographically Weighted Regression:
376 A Method for Exploring Spatial Nonstationarity. *Geogr. Anal.* 28, 281–298.

377 <https://doi.org/https://doi.org/10.1111/j.1538-4632.1996.tb00936.x>

378 Calkin, D.E., Thompson, M.P., Finney, M.A., 2015. Negative consequences of positive
379 feedbacks in us wildfire management. *For. Ecosyst.* 2, 1–10.

380 <https://doi.org/10.1186/s40663-015-0033-8>

381 Cascio, W.E., 2018. Wildland Fire Smoke and Human Health. *Sci. Total Environ.* 624, 586–595.



- 382 <https://doi.org/10.1016/j.scitotenv.2017.12.086>.
- 383 CDC, 2011. Asthma in the US. CDC Vital Signs 1–4.
- 384 Chu, Y., Liu, Y., Li, X., Liu, Z., Lu, H., Lu, Y., Mao, Z., Chen, X., Li, N., Ren, M., Liu, F., Tian,
385 L., Zhu, Z., Xiang, H., 2016. A review on predicting ground PM_{2.5} concentration using
386 satellite aerosol optical depth. *Atmosphere (Basel)*. 7, 129.
387 <https://doi.org/10.3390/atmos7100129>
- 388 Coogan SCP, Robinne F-N, Jain P, Flannigan MD. 2019. Scientists’ warning on wildfire — a
389 Canadian perspective. *Can. J. For. Res.* 49(9): 1015-1023.
- 390 Donkelaar, A. Van, Martin, R. V, Park, R.J., 2006. Estimating ground-level PM_{2.5} using
391 aerosol optical depth determined from satellite remote sensing. *J. Geophys. Res. Atmos.*
392 111. <https://doi.org/10.1029/2005JD006996>
- 393 Donkelaar, A. Van, Martin, R. V, Spurr, R.J.D., Burnett, R.T., 2015. High-Resolution Satellite-
394 Derived PM_{2.5} from Optimal Estimation and Geographically Weighted Regression over
395 North America. *Environ. Sci. Technol.* 49, 10482–10491.
396 <https://doi.org/10.1021/acs.est.5b02076>
- 397 Dreessen, J., Sullivan, J., Delgado, R., 2016. Observations and impacts of transported Canadian
398 wildfire smoke on ozone and aerosol air quality in the Maryland region on June 9–12, 2015.
399 *J. Air Waste Manag. Assoc.* 66, 842–862. <https://doi.org/10.1080/10962247.2016.1161674>
- 400 ESA, 2017. ESA. Land Cover CCI Product User Guide Version 2. Tech. Rep.
- 401 Fotheringham, A.S., Charlton, M.E., Brunson, C., 1998. Geographically weighted regression: a
402 natural evolution of the expansion method for spatial data analysis. *Environ. Plan. A* 30,



- 403 1905–1927.
- 404 Fotheringham, S.A., Brunson, C., Charlton, M., 2003. Geographically Weighted Regression :
405 The Analysis of Spatially Varying Relationships, John Wiley and Sons.
- 406 Freeborn, P.H., Wooster, M.J., Roy, D.P., Cochrane, M.A., 2014. Quantification of MODIS fire
407 radiative power (FRP) measurement uncertainty for use in satellite-based active fire
408 characterization and biomass burning estimation. *Geophys. Res. Lett.* 41, 1988–1994.
409 <https://doi.org/10.1002/2013GL059086>.
- 410 Gu, Y., 2019. Estimating PM_{2.5} Concentrations Using 3 km MODIS AOD Products : A Case
411 Study in British Columbia , Canada. University of Waterloo.
- 412 Gupta, P., Christopher, S.A., 2009a. Particulate matter air quality assessment using integrated
413 surface, satellite, and meteorological products: 2. A neural network approach. *J. Geophys.*
414 *Res. Atmos.* 114, 1–14. <https://doi.org/10.1029/2008JD011497>
- 415 Gupta, P., Christopher, S.A., 2009b. Particulate matter air quality assessment using integrated
416 surface , satellite , and meteorological products : Multiple regression approach. *J. Geophys.*
417 *Res. Atmos.* 114, 1–13. <https://doi.org/10.1029/2008JD011496>
- 418 Hall, E.S., Kaushik, S.M., Vanderpool, R.W., Duvall, R.M., Beaver, M.R., Long, R.W.,
419 Solomon, P.A., 2013. Integrating Sensor Monitoring Technology into Current Air
420 Pollution Regulatory Support Paradigm: Practical Considerations. *Am. J. Environ. Eng* 4,
421 147–154. <https://doi.org/10.5923/j.ajee.20140406.02>
- 422 Hessburg, P.F., Churchill, D.J., Larson, A.J., Haugo, R.D., Miller, C., Spies, T.A., North, M.P.,
423 Povak, N.A., Belote, R.T., Singleton, P.H., Gaines, W.L., Keane, R.E., Aplet, G.H.,



- 424 Stephens, S.L., Morgan, P., Bisson, P.A., Rieman, B.E., Salter, R.B., Reeves, G.H., 2015.
425 Restoring fire-prone Inland Pacific landscapes: seven core principles. *Landsc. Ecol.* 30,
426 1805–1835. <https://doi.org/10.1007/s10980-015-0218-0>
- 427 Hoff, R.M., Christopher, S.A., 2009. Remote Sensing of Particulate Pollution from Space : Have
428 We Reached the Promised Land ? *J. Air Waste Manage. Assoc.* 59, 645–675.
429 <https://doi.org/10.3155/1047-3289.59.6.645>
- 430 Hu, X., Waller, L.A., Al-Hamdan, M.Z., Crosson, W.L., Estes, M.G., Estes, S.M., Quattrochi,
431 D.A., Sarnat, J.A., Liu, Y., 2013. Estimating ground-level PM_{2.5} concentrations in the
432 southeastern U.S. using geographically weighted regression. *Environ. Res.* 121, 1–10.
433 <https://doi.org/10.1016/j.envres.2012.11.003>
- 434 Hu, Z., 2009. Spatial analysis of MODIS aerosol optical depth, PM_{2.5}, and chronic coronary
435 heart disease. *Int. J. Health Geogr.* 8, 1–10. <https://doi.org/10.1186/1476-072X-8-27>
- 436 Hubbell, B.J., Crume, R. V., Evarts, D.M., Cohen, J.M., 2010. Policy Monitor: Regulation and
437 progress under the 1990 Clean Air Act Amendments. *Rev. Environ. Econ. Policy* 4, 122–
438 138. <https://doi.org/10.1093/reep/rep019>
- 439 Hystad, P., Demers, P.A., Johnson, K.C., Brook, J., Van Donkelaar, A., Lamsal, L., Martin, R.,
440 Brauer, M., 2012. Spatiotemporal air pollution exposure assessment for a Canadian
441 population-based lung cancer case-control study. *Environ. Heal. A Glob. Access Sci.*
442 *Source* 11, 1–22. <https://doi.org/10.1186/1476-069X-11-22>
- 443 J.A.Gillies, W.G.Nickling, G.H.Mctainsh, 1996. Dust concentration s and particle-size
444 characteristics of an intense dust haze event: inland delta region. *Atmos. Environ.* 30, 1081–
445 1090.



- 446 Kearns, M., Ron, D., 1999. Algorithmic stability and sanity-check bounds for leave-one-out
447 cross-validation. *Neural Comput.* 11, 1427–1453.
448 <https://doi.org/10.1162/089976699300016304>
- 449 Kollanus, V., Tiittanen, P., Niemi, J. V., Lanki, T., 2016. Effects of long-range transported air
450 pollution from vegetation fires on daily mortality and hospital admissions in the Helsinki
451 metropolitan area, Finland. *Environ. Res.* 151, 351–358.
452 <https://doi.org/10.1016/j.envres.2016.08.003>
- 453 Loader, C.R., 1999. BANDWIDTH SELECTION: CLASSICAL OR PLUG-IN? *Ann. Stat.* 27,
454 415–438.
- 455 Lyapustin, A., Wang, Y., Korkin, S., Huang, D., 2018. MODIS Collection 6 MAIAC Algorithm.
456 *Atmos. Meas. Tech.* 11, 5741–5765. <https://doi.org/10.5194/amt-2018-141>
- 457 Ma, Z., Hu, X., Huang, L., Bi, J., Liu, Y., 2014. Estimating ground-level PM_{2.5} in china using
458 satellite remote sensing. *Environ. Sci. Technol.* 48, 7436–7444.
459 <https://doi.org/10.1021/es5009399>
- 460 Meixner, T., Wohlgemuth, P., 2004. Wildfire Impacts on Water Quality. *J. Wildl. Fire* 13, 27–
461 35.
- 462 Melillo, J.M., Richmond, T., Yohe, G.W., 2014. Climate Change Impacts in the United States.
463 *Third Natl. Clim. Assess.* 52. <https://doi.org/10.7930/J0Z31WJ2>.
- 464 Miller, D.J., Sun, K., Zondlo, M.A., Kanter, D., Dubovik, O., Welton, E.J., Winker, D.M.,
465 Ginoux, P., 2011. Assessing boreal forest fire smoke aerosol impacts on U.S. air quality: A
466 case study using multiple data sets. *J. Geophys. Res. Atmos.* 116.



- 467 <https://doi.org/10.1029/2011JD016170>
- 468 Mirzaei, M., Bertazzon, S., Couloigner, I., 2018. Modeling Wildfire Smoke Pollution by
469 Integrating Land Use Regression and Remote Sensing Data : Regional Multi-Temporal
470 Estimates for Public Health and Exposure Models. *Atmosphere (Basel)*. 9, 335.
471 <https://doi.org/10.3390/atmos9090335>
- 472 Munoz-alpizar, R., Pavlovic, R., Moran, M.D., Chen, J., Gravel, S., Henderson, S.B., Sylvain,
473 M., Racine, J., Duhamel, A., Gilbert, S., Beaulieu, P., Landry, H., Davignon, D., Cousineau,
474 S., Bouchet, V., 2017. Multi-Year (2013–2016) PM_{2.5} Wildfire Pollution Exposure over
475 North America as Determined from Operational Air Quality Forecasts. *Atmosphere (Basel)*.
476 8, 179. <https://doi.org/10.3390/atmos8090179>
- 477 Navarro, K.M., Schweizer, D., Balmes, J.R., Cisneros, R., 2018. A review of community smoke
478 exposure from wildfire compared to prescribed fire in the United States. *Atmosphere*
479 *(Basel)*. 9, 1–11. <https://doi.org/10.3390/atmos9050185>
- 480 Samet, J.M., 2011. The clean air act and health - A clearer view from 2011. *N. Engl. J. Med.*
481 365, 198–201. <https://doi.org/10.1056/NEJMp1103332>
- 482 Sapkota, A., Symons, J.M., Kleissl, J., Wang, L., Parlange, M.B., Ondov, J., Breysse, P.N.,
483 Diette, G.B., Eggleston, P.A., Buckley, T.J., 2005. Impact of the 2002 Canadian forest fires
484 on particulate matter air quality in Baltimore City. *Environ. Sci. Technol.* 39, 24–32.
485 <https://doi.org/10.1021/es035311z>
- 486 Stephens, S.L., 2005. Forest fire causes and extent on United States Forest Service lands. *Int. J.*
487 *Wildl. Fire* 14, 213–222. <https://doi.org/10.1071/WF04006>



- 488 U.S. Environmental Protection Agency, 2019. Particulate Matter (PM_{2.5}) Trends.
- 489 You, W., Zang, Z., Pan, X., Zhang, L., Chen, D., 2015. Estimating PM_{2.5} in Xi'an, China using
490 aerosol optical depth: A comparison between the MODIS and MISR retrieval models. *Sci.*
491 *Total Environ.* 505, 1156–1165. <https://doi.org/10.1016/j.scitotenv.2014.11.024>
- 492 You, W., Zang, Z., Zhang, L., Li, Y., Pan, X., Wang, W., 2016. National-scale estimates of
493 ground-level PM_{2.5} concentration in China using geographically weighted regression based
494 on 3 km resolution MODIS AOD. *Remote Sens.* 8. <https://doi.org/10.3390/rs8030184>
- 495 Zhang, H., Hoff, R.M., Engel-Cox, J.A., 2009. The relation between moderate resolution
496 imaging spectroradiometer (MODIS) aerosol optical depth and PM_{2.5} over the United
497 States: A geographical comparison by U.S. Environmental Protection Agency regions. *J.*
498 *Air Waste Manag. Assoc.* 59, 1358–1369. <https://doi.org/10.3155/1047-3289.59.11.1358>
- 499 Zheng, C., Zhao, C., Zhu, Y., Wang, Y., Shi, X., Wu, X., Chen, T., Wu, F., Qiu, Y., 2017.
500 Analysis of influential factors for the relationship between PM_{2.5} and AOD in Beijing.
501 *Atmos. Chem. Phys.* 17, 13473–13489. <https://doi.org/10.5194/acp-17-13473-2017>
- 502 Zhu, Y., Hinds, W.C., Kim, S., Sioutas, C., 2002. Concentration and size distribution of ultrafine
503 particles near a major highway. *J. Air Waste Manag. Assoc.* 52, 1032–1042.
504 <https://doi.org/10.1080/10473289.2002.10470842>
- 505 Zou, B., Pu, Q., Bilal, M., Weng, Q., Zhai, L., Nichol, J.E., 2016. High-resolution Satellite
506 Mapping of Fine Particulates Based on Geographically Weighted Regression. *Ieee Geosci.*
507 *Remote Sens. Lett.* 13, 495–499.
- 508
- 509



510 Table 1. Datasets used in the study with sources.

511

	Data /Model	Sensor	Spatial Resolution	Temporal Resolution	Accuracy
1	Surface PM2.5	TEOM	Point data	daily	±5~10%
2	Mid visible aerosol optical depth (AOD)	MAIAC_ MODIS	1km	daily	66% compared to AERONET
3	Fire Radiative Power (FRP)	Terra/Aqua- MODIS	1km	daily	± 7%
4	ECMWF (Meteorological variables)		0.25 degree	hourly	
5	Land cover	MERIS SR	300m	Annual	
6	Population		5km		

512 1) <https://www.epa.gov/outdoor-air-quality-data>

513 2) <https://earthdata.nasa.gov/>

514 3) <https://earthdata.nasa.gov/>

515 4) <https://www.ecmwf.int/en/forecasts>

516 5) <https://www.esa-landcover-cci.org>

517 6) <https://sedac.ciesin.columbia.edu/data/collection/gpw-v4>

518

519



520

521 Table 2. Total FRP in Canada and Northwestern US in August of Different Years (unit: 10⁴

522

MW)

Year	2010	2011	2012	2013	2014	2015	2016	2017	2018
CA	148.24	4.84	19.93	70.54	107.78	10.39	4.6	307.3	542.99
NW US	16.41	42.84	320.39	192.06	67.01	339.58	112.9	195.64	296.91

523

524

525 Table 3. Mean PM_{2.5} from August 9th to August 25th in 2018 and 2011 of different states

State	2018	2011
WA	47.0	5.874
OR	33.10	4.97
ID	26.26	6.79
MT	25.86	7.55
CA	21.22	7.66
ND	20.20	7.41
NV	17.92	5.51
SD	17.72	7.31
MN	16.41	6.27
WY	15.71	6.59
NE	15.69	6.81
UT	14.87	6.51
IA	14.73	7.87
KS	14.13	6.84
AR	13.92	11.59
WI	13.70	6.26
OK	13.53	9.26
MO	13.25	9.64
LA	13.24	13.07
IL	12.98	11.36
MS	12.86	13.67
CO	12.31	6.07
MI	11.97	6.82
TX	11.70	9.27
TN	11.66	14.39
AL	11.65	14.97



IN	11.50	12.51
KY	11.02	13.19
DC	10.65	13.16
NJ	10.56	9.76
DE	10.37	11.16
GA	10.22	14.02
CT	10.20	9.74
OH	10.14	11.84
FL	10.13	10.68
MD	10.07	12.59
NM	9.842	6.03
SC	9.829	12.66
PA	9.75	12.64
NC	9.67	12.44
RI	9.633	8.602
MA	9.56	9.413
VA	9.38	13.74
NY	9.33	9.731
WV	9.28	13.58
NH	9.11	9.33
AZ	9.08	7.00
VT	8.96	9.34
ME	7.972	10.52

526

527

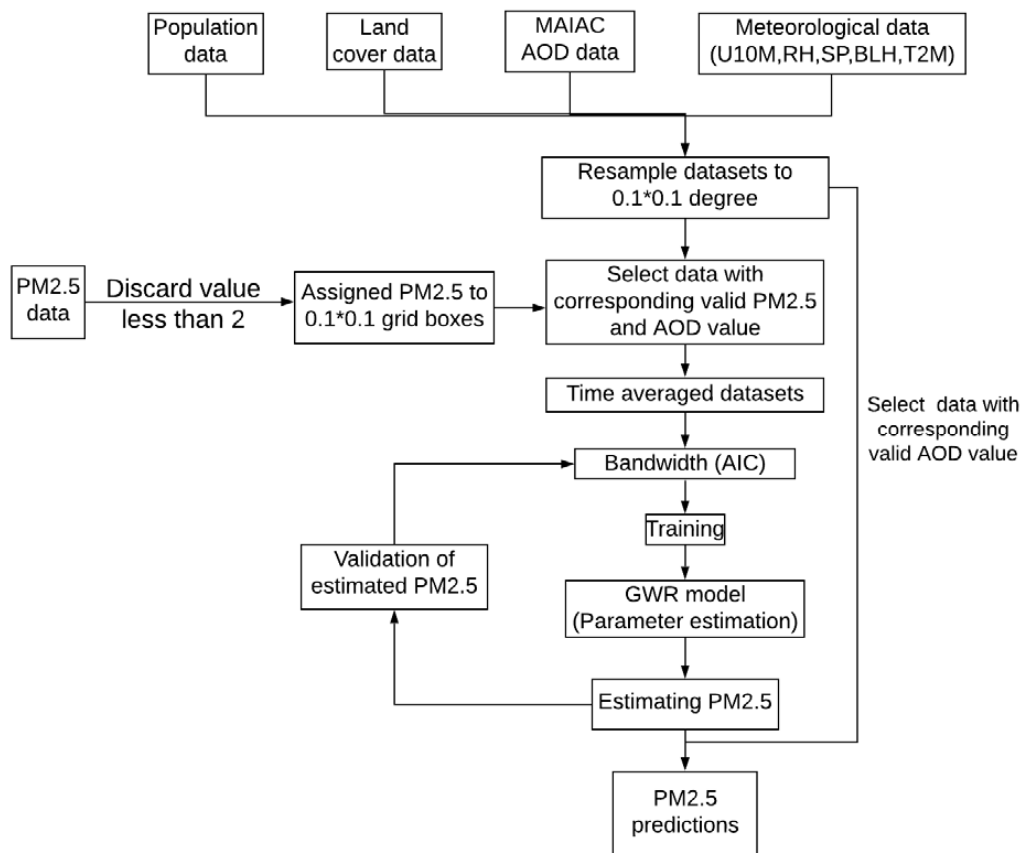
528

529

530

531

532



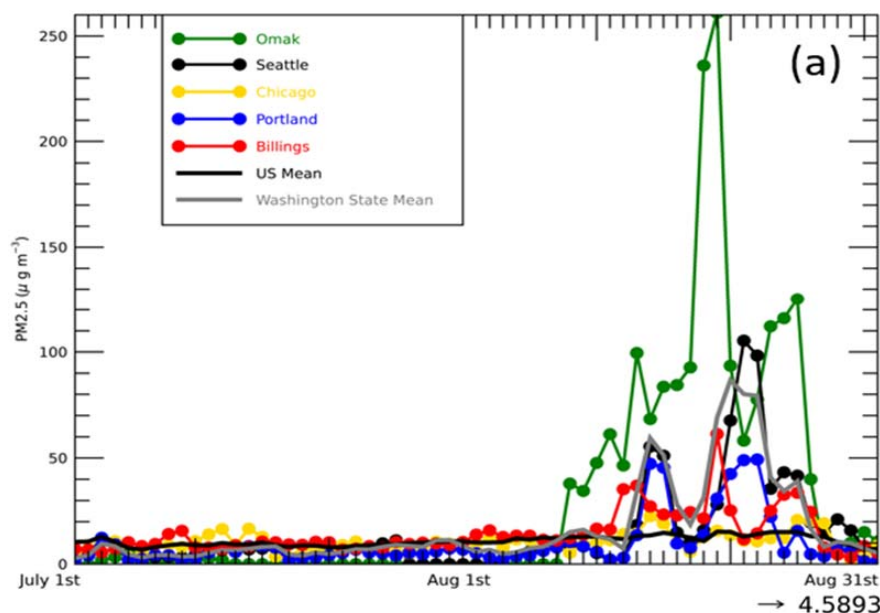
533

534 Figure 1. Flow chart for the Geographically Weighted Regression model used. All satellite,

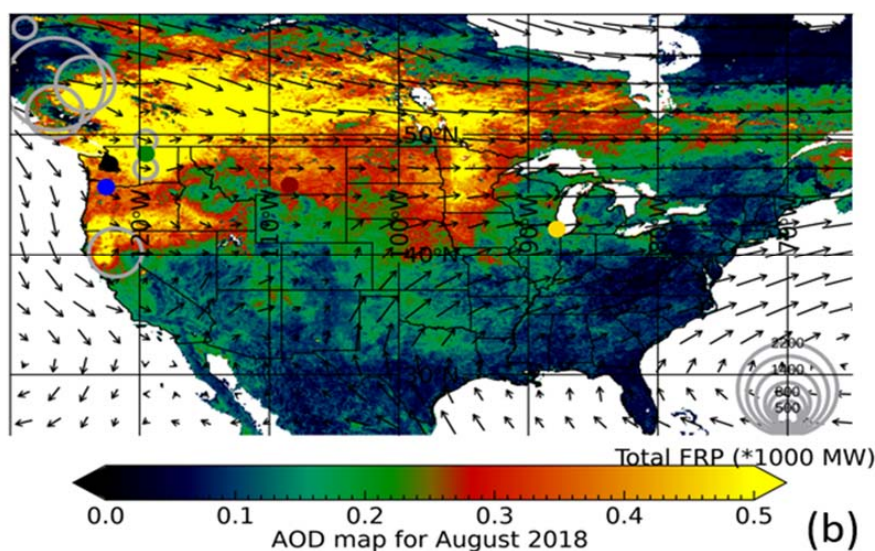
535 ground, meteorological data are gridded to 0.1 by 0.1 degrees.

536

537

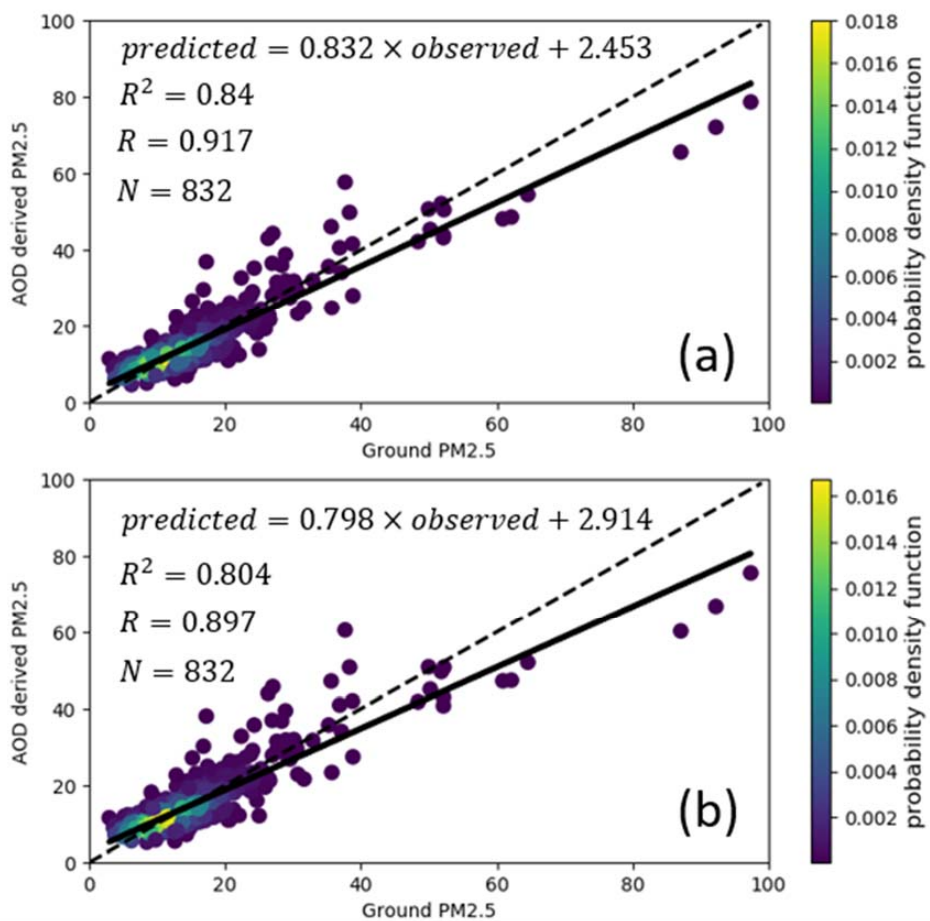


538



539

540 Figure 2. (a) Variations of EPA ground observed PM_{2.5} in different cities from July to August
541 2018 (Omak-Washington, Seattle-Washington, Chicago-Illinois, Portland-Oregon, Billings-
542 Montana). Black line without markers shows the mean variation of the whole US stations and the
543 grey line without markers shows the mean variation of stations in Washington state. (b) Mean
544 MAIAC satellite AOD distribution from August 9th to August 25th, 2018. AOD values equal or
545 larger than 0.5 are shown as the same color (yellow). Also shown are circles with Fire Radiative
546 Power (FRP). Black arrow shows the wind direction and the length of it represents the wind
547 speed. The round spots of different colors on the map show the locations of the five selected
548 cities (green-Omak, black-Seattle, yellow-Chicago, blue-Portland, red-Billings).



549

550 Figure 3. Results of model fitting and cross validation for GWR model for the entire US region
551 averaged from August 9th to August 25th, 2018. (a) GWR model fitting results (b) GWR model
552 LOOCV results. The dash line is the 1:1 line as reference and the black line shows the regression
553 line. The color of the scatter plots represents the probability density function which provides a
554 relative likelihood that the value of the random variable would equal a certain sample.

555

556

557

558

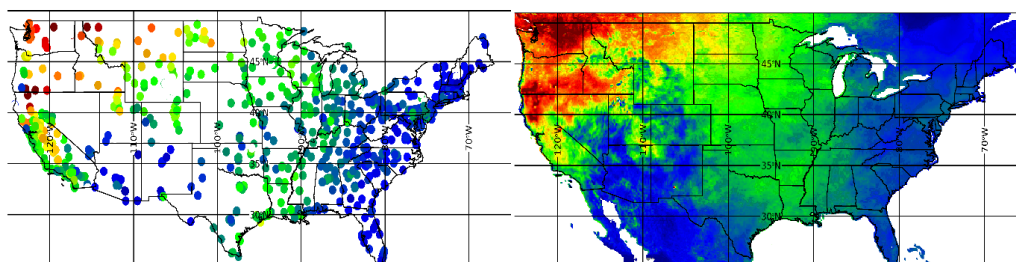
559

560

561

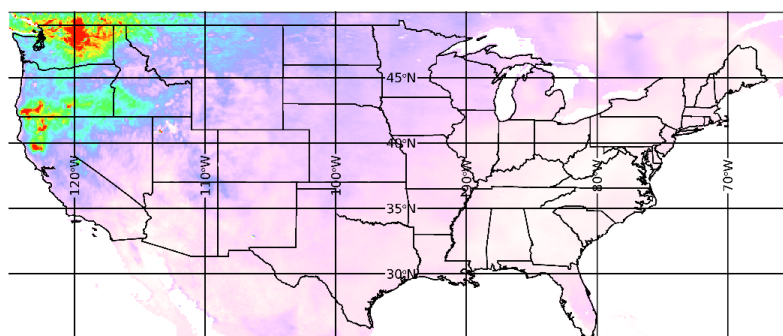
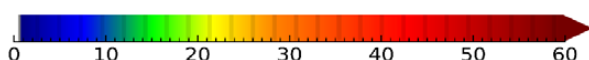


562



563

564



565

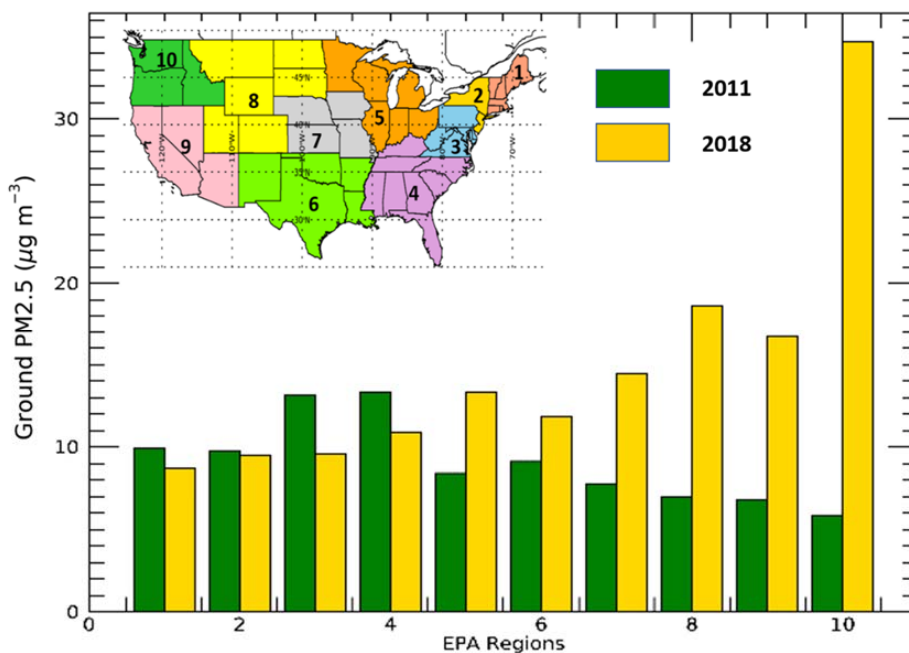
D-PM2.5 map between 2018 and 2011 August

566 Figure 4. (a) EPA ground observed PM2.5 distribution over the US averaged from August 9th to
567 August 25th, 2018. (b) GWR predicted 17-day mean PM2.5 distribution. (c) Difference map of
568 predicted ground PM2.5 of the 17-day mean values between 2018 and 2011. PM2.5 values equal
569 or larger than $30 \mu\text{g m}^{-3}$ are shown as the same color (red). Note that the D-PM2.5 has a
570 different color scale to make the negative values more apparent (blue).
571

572



573



574

575 Figure 5. Mean PM_{2.5} of EPA regions from August 9th to August 25th in 2011 and 2018. Inset
576 shows the map of 10 EPA regions in different colors. Yellow column represents the 2018 mean
577 PM_{2.5} and green column represents for 2011 mean PM_{2.5}.

578

579